Measurement of Double-Layer Forces at the Polymer Film/Electrolyte Interfaces Using Atomic Force Microscopy: Concentration and Potential-Dependent Interactions

Jian Wang,[†,‡] Stephen W. Feldberg,[§] and Allen J. Bard*[,†]

Department of Chemistry and Biochemistry, The University of Texas at Austin, Austin, Texas 78712, and Brookhaven National Laboratory, Upton, New York 11973-5000

Received: June 20, 2002; In Final Form: July 31, 2002

The forces between colloidal probes and several polymer films were measured by atomic force microscopy in the presence of a series of electrolyte solutions. For Nafion films using a negatively charged silica tip, a repulsive force was obtained at different concentrations of $NaClO_4$. A similar result was obtained for an anion exchange membrane with a positively charged probe. Derjaguin−Landau−Verwey−Overbeek (DLVO) theory was employed to calculate the surface potential and hence, the surface charge. The surface charge density ($\sim 0.3 \mu C/cm^2$) was independent of electrolyte concentration. The slope for plot of potential drop vs $\ln[c^s]$ was ~0.020 V. A theoretical treatment based on GCS theory was employed to account for the above results. For a poly(vinylferrocene) (PVF) film, potential-dependent force curves were obtained, which were qualitatively different from that previously reported for an electronically conducting polymer film electrode.[1]

1. Introduction

We discuss here the nature of the diffuse double layer (ddl) at the interface between several types of polymers and dilute aqueous electrolytes as determined by atomic force microscopy (AFM) measurements. The electrical double layer at the solid/electrolyte interface is of interest for many materials, such as electrodes and colloids, and has been the subject of numerous studies.[2−6] A number of experimental techniques have been employed to characterize solid/liquid interfaces and electrical double layer. AFM force measurements based on colloidal probe attached to a cantilever tip is a recent powerful technique for such investigations.[7,8] An advantage of this technique is that it can be used with a wide variety of substrates without regard to size, structure, or transparency. Another advantage is that it can easily combine with electrochemistry, which makes it possible to study surface forces of electrodes at different potentials.[9,10] These kinds of studies are difficult with the surface force apparatus.[11] Over the past decade a number of different systems, such as silica (glass),[7,12] Al_2O_3,[13] gold,[14] copper,[15] mica,[16] TiO_2,[17,18] self-assembled monolayer,[19,20] surfactant,[21] DNA,[22,23] oil droplet,[24] polypropylene,[25] polystyrene,[26] and nanoparticles[27] have been studied using the AFM technique.

Double layers are also of interest at certain polymers, such as polyelectrolytes (e.g., ion exchange membranes) and electroactive polymer films on electrode surfaces. In a previous study,[1] conjugated electronically conducting polymers (polypyrrole, polythiophene) were studied using the in situ AFM/electrochemistry technique. We found that the conjugated conducting polymer electrodes were qualitatively different from metal and semiconductor electrodes, in that there appeared to be complete internal charge compensation in the polymer film upon charging (doping) and no diffuse double layer was found at the polymer film/solution interface. However, Campbell, and Hillier[28] recently reported that a sulfonated polyaniline film, a conducting polymer with fixed charges, showed force curves indicating either repulsive or attractive behavior, depending upon the potential of the glassy carbon substrate. In this paper, we report results for two ion exchange membranes (Nafion and an anion exchange membrane) and redox polymer, poly(vinylferrocene) (PVF) at different levels of oxidation. We show, in contrast to the electronically conducting polymers, that diffuse double layers are present with these, as determined by AFM repulsive force measurements, the surface charge is independent of electrolyte concentration (c^s) and the slope for plot of potential drop vs $\ln[c^s]$ is ~0.020 V. A theoretical treatment based on Gouy−Chapman-Stern (GCS) theory is employed to account for the above results.

2. Experimental Section

2.1 Materials. *(a) Reagents.* $NaClO_4$, $HClO_4$, Nafion 117 (5% in alcohol and water) (Aldrich, Milwaukee, WI), and poly(vinylferrocene) (MW ≈ 50 000, Polysciences, Warrington, PA) were reagent grade chemicals and used as received. The anion exchange membrane was a quaternary ammonium polystyrene resin. Solutions were prepared with 18 MΩ deionized water (Milli-Q Plus, Millipore Corp., Bedford, MA). Immediately before use, the solutions were deaerated with argon for 20 min.

(b) Film and Substrate Preparation. Silica substrates were prepared from commercial glass microscope slides (Fisher Scientific, Pittsburgh, PA). Before each experiment, the silica substrates were cleaned in piranha solution (a mixture of 70% H_2SO_4 and 30% H_2O_2) at ~90 °C for 10 min. (*Caution: piranha solution reacts violently with organic compounds and should be handled carefully.*) Nafion films were spin-coated from a 1% aqueous solution onto a pre-cleaned Au substrate. The film thickness was roughly 200 nm. Gold substrates were prepared by vacuum evaporation of high-purity gold (99.999%) onto a cleaned silicon (100) wafer that was precoated with chromium to improve adhesion (typically, 200 nm Au, 10 nm Cr). The anion exchange membrane was used directly without any substrate. PVF films were spin-coated onto either a vacuum

[†] The University of Texas at Austin.
[‡] Present address: Department of Chemistry, Boston University, Boston, MA 02215.
[§] Brookhaven National Laboratory.

10.1021/jp026350k CCC: $22.00
Published on Web 09/14/2002

evaporated Au substrate, or as described earlier.[9] In the latter, the gold substrate electrodes were prepared by gluing a 2-mm-diameter gold wire (99.99%, Aldrich) with epoxy (Torr Seal, Varian) into a 3-mm-diameter hole in a 12-mm-diameter × 4-mm-thick glass disk. The gold/glass surface was polished to optical smoothness with successive Carbimet papers and Al_2O_3 powder (1 μm, 0.3 μm, 0.05 μm) (Buehler, Lake Bluff, IL). Immediately prior to use, the sample was polished with 0.05 μm Al_2O_3 for several min, rinsed with water and dried under argon.

(c) *Probe preparation.* Force curves were acquired using a standard Si_3N_4 AFM cantilever (Digital Instruments, Santa Barbara, CA) that has been modified with either a silica sphere (Polyscience, Warrington, PA) with diameter of 10−20 μm or an amino-terminated polymer sphere (PAN06/3627, Bangs Lab Inc., Fishers, IN) with a diameter of 9.1 μm. A sphere was attached to the very end of the AFM cantilever using epoxy resin (Epon 1002, Shell, Houston, TX) and an optical microscope (Olympus, Model BHTU, Tokyo, Japan) with a three-dimensional micropositioning stage. Immediately prior to use, the tip was rinsed with ethanol and water and blown dry with argon.

2.2 Electrochemistry. For in situ electrochemical measurements, experiments were carried out in an AFM liquid cell (Digital Instruments, Santa Barbara, CA) with Teflon tubing inlets and outlets. A three-electrode design was used in electrochemical measurements with the PVF film electrode serving as the working electrode, a Pt counter electrode, and an Ag/AgCl wire immersed in the solution as a reference electrode. All electrode potentials are cited with respect to this Ag/AgCl wire reference. Electrochemical control of the cell was carried out with a CHI-660 electrochemical work station (CH Instruments, Austin, TX) under computer control.

2.3 AFM Force Measurement. All force measurements were performed with a Nanoscope III AFM (Digital Instruments) equipped with a piezo scanner having a maximum scan range of 15 × 15 × 2 μm. The AFM force measuring technique is well documented and the experimental details have been described elsewhere.[9] Briefly, the raw data giving the tip deflection vs substrate displacement were converted to normalized force (force/radius, F/R) vs tip−substrate separation curves for further analysis with the knowledge of the scanner calibration, cantilever spring constant, and tip radius. The spring constant of the sphere-modified cantilever was 0.35−0.65 N/m. Derjaguin−Landau−Verwey−Overbeek (DLVO) theory[29−32] was employed to calculate the surface potential. The electrical double layer interaction energy was calculated for the constant-charge limit of the complete nonlinear Poisson−Boltzmann equation using the method of Hillier et al.,[9] who used a finite element discretization of the equation with linear basis functions.

The surface charge, σ^M, was calculated from the surface potential, ϕ_2 (the potential at the plane of closest approach vs the bulk solution), measured by the AFM technique by the following formula[33]

$$\sigma^m = -\sigma^s = \sqrt{8RT\epsilon^s\epsilon_o c_s}\sinh\left[\frac{F}{2RT}\phi_2\right] \qquad (1)$$

where ϵ^s is the dielectric constant of the solution, ϵ_o is the permittivity of free space (8.854×10^{-14} $CV^{-1}cm^{-1}$), c^s is the concentration of electrolyte in the solution phase and F, R, and T have their usual meanings.

3. Results and Discussion

3.1 Ion Exchange Films. *3.1.1 AFM Images.* Figures 1 and 2 show the AFM images of a Nafion film[34] and an anion exchange membrane, respectively. For the Nafion, a very smooth film was obtained with an RMS roughness value of 1.49 nm over the 1 × 1 μm area. The anion exchange membrane was a little rougher, with a mean roughness of 2.20 nm over a 1 × 1 μm area.

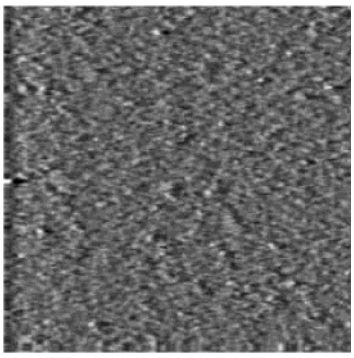

Figure 1. Atomic force microscopy image of Nafion film. Scan area: 15 × 15 μm, Z-height: 50 nm.

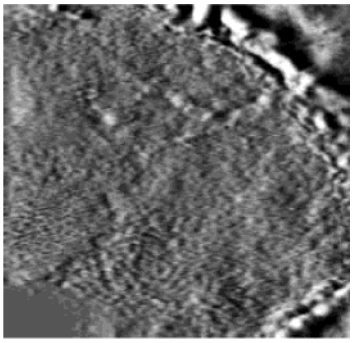

Figure 2. Atomic force microscopy image of anion exchange membrane. Scan area: 15 × 15 μm, Z-height: 200 nm.

3.1.2 Characterization of a Positively Charged AFM Probe. The passive cantilever used to measure forces with the standard AFM is limited by the nature of the AFM probe. In the presence of purely repulsive forces, the cantilever deflection provides a complete indication of the interaction up to surface contact. The most commonly used colloidal probe for AFM force measurements is a silica sphere. Because the silica is negatively charged in electrolyte solutions of pH > 3, the silica probe can be used to characterize negatively charged surfaces under these conditions. For positively charged surfaces, attractive forces that exceed a maximum value lead to instability (jump to contact) and make the cantilever less useful in the accurate measurement of attractive forces. Therefore, a positively charged probe is more useful in the measurement of positively charged surfaces.

There are a number of possible ways to prepare positively charged AFM probes, e.g., surface modification of the silica sphere, surface adsorption on the silica sphere, or direct use of a positively charged polymer sphere. In this work, we used the latter strategy, that is, to modify the AFM cantilever with a positively charged polymer sphere. The sphere used was an amino-terminated polymer sphere (PAN06/3627, Bangs Lab Inc., Fishers, IN). Because the surface properties of amino group are very sensitive to solution pH, it is important to precisely control the pH value of the solutions to get the desired surface properties. Figure 3 shows a test of the probe by measuring the force between the polymer sphere-modified AFM probe and a glass substrate in a solution of two different pH-values. In 10^{-3} M NaCl at pH 6, both the probe and the substrate were negatively charged and therefore a repulsive force curve was

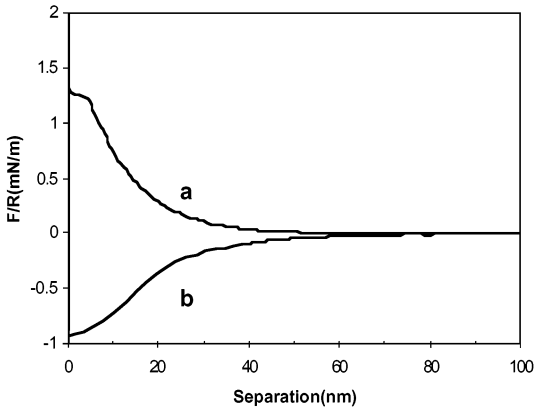

Figure 3. Force between an amino-terminated polymer sphere modified AFM probe and glass substrate at different solutions. (a) 10^{-3} M NaCl; (b) 10^{-4} M $HClO_4$.

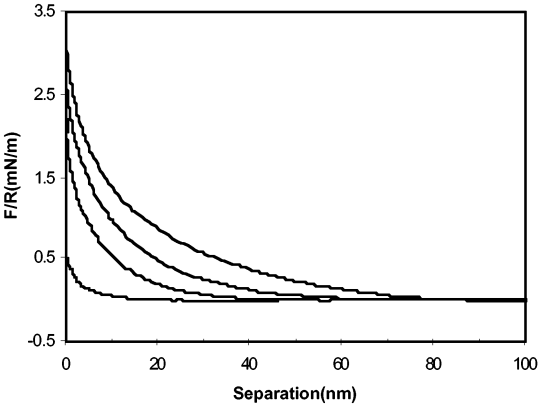

Figure 4. Force between a negatively charged silica sphere and the Nafion film in $NaClO_4$ solution as a function of electrolyte concentration. The curves correspond to electrolyte concentrations, from bottom to top, 10^{-2} M, 10^{-3} M, 3×10^{-4} M, and 10^{-4} M.

obtained. In 10^{-4} M $HClO_4$ of pH 4, an attractive force was obtained. Because the glass substrate is still negatively charged in a solution of pH 4, the polymer sphere modified AFM probe is clearly positive under these conditions.

3.1.3 Concentration-Dependent Interactions. Figure 4 shows the force curves between a negatively charged silica sphere and a Nafion film as a function of electrolyte concentration. Repulsive force curves were obtained for all cases. The measured forces decayed exponentially with distance, and both the decay lengths and potentials decreased with concentration, as expected. Nafion is a perfluoronated sulfonate polymer and is negatively charged in neutral solutions, so the electrostatic interaction between the negatively charged silica sphere-modified AFM probe and Nafion film is repulsive. Similar behavior was also found for the interaction between a polymer sphere-modified positively charged AFM probe and a positively charged anion exchange membrane (Figure 5).

To calculate the surface potential (ϕ_2) of the polymer film, the force data were compared to theoretical predictions of the forces between dissimilarly charged surfaces obtained by solving the complete nonlinear Poisson−Boltzmann equation.[9] For this procedure, the surface potential of the silica sphere and the Hamaker constant, A_H, between the silica sphere and polymer film at different concentrations must be known. The surface potential of the silica sphere as a function of electrolyte concentration was determined by measuring forces between the sphere and a silica (glass) substrate, as described earlier.[35] The surface potentials for silica sphere obtained in our experiments

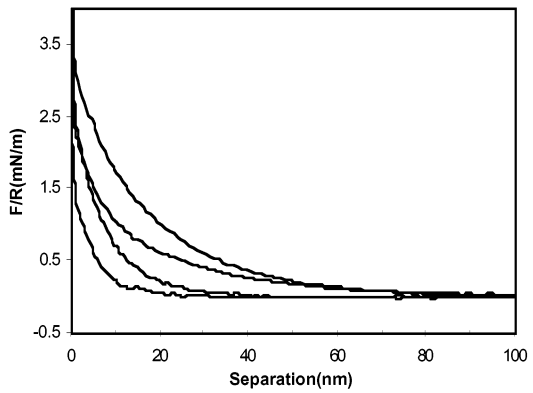

Figure 5. Force between a positively charged polymer-sphere modified probe and positively charged anion exchange membrane in 10^{-4} M $HClO_4$ + X M $NaClO_4$ solution of different concentrations. The curves correspond to total electrolyte concentrations, from bottom to top, 10^{-2} M, 10^{-3} M, 3×10^{-4} M, and 10^{-4} M.

were −20, −40, −60, and −90 mV in $NaClO_4$ solutions with concentrations of 10^{-2}, 10^{-3}, 3×10^{-4}, and 10^{-4} M, respectively. The Hamaker constant was estimated to be 1.0×10^{-20} J for the silica-polymer film interaction. In Figure 6, we show the results of theoretical curves fit to experimental force data with $NaClO_4$ solutions of different concentrations. The dotted curve is experimental data. The solid curve is calculated for the model with boundary conditions constrained to a constant surface charge at both the probe and the substrate. The constant surface charge condition was previously shown to fit experimental results better than the constant surface potential condition.[9] Table 1 lists the surface potential and surface charge of a Nafion film in $NaClO_4$ solutions of different concentration. The surface potential increases as the concentration decreases. The surface charge density ($\sim -0.32 \pm 0.01$ μC/cm^2), however, is independent of solution concentration. This result is somewhat counterintuitive, since as the electrolyte concentration increases, one might expect that there would be more counterions penetrating into the film to compensate the fixed charge, therefore reducing the surface charge.

For the anion exchange membrane, the force data were also compared to theoretical predictions of the forces between dissimilarly charged surfaces obtained from the complete nonlinear Poisson−Boltzmann equation.[9] The Hamaker constant was again estimated to be 1.0×10^{-20} J. The surface potential of the amino-terminated polymer sphere as a function of electrolyte concentration in a solution of pH 4 was estimated to 25, 55, 70, and 90 mV. This estimation was based on the surface properties of surface hydroxyl group, so it may not be very accurate. On the basis of these estimates, the surface potential and surface charge of anion exchange membrane in solutions of pH 4 as a function of electrolyte concentration were also calculated and listed in Table 2. The behavior for anion exchange membrane is similar to that of the Nafion film, i.e., the surface potential increases as the concentration decreases and the surface charge density ($\sim 0.36 \pm 0.02$ μC/cm^2) is independent of solution concentration.

3.2 PVF Films. Figure 7 shows the AFM image of a PVF film. The film is very smooth with an RMS roughness of 0.67 nm over a 1×1 μm area. The cyclic voltammogram (CV) of PVF film is shown in Figure 8. The electrochemical responses of electroactive polymer films are frequently different for the first redox cycles.[36] This effect was found in this work and became negligible after the preconditioning step (or "breaking in") of several cycles. The CV showed here is the stable CV after preconditioning.

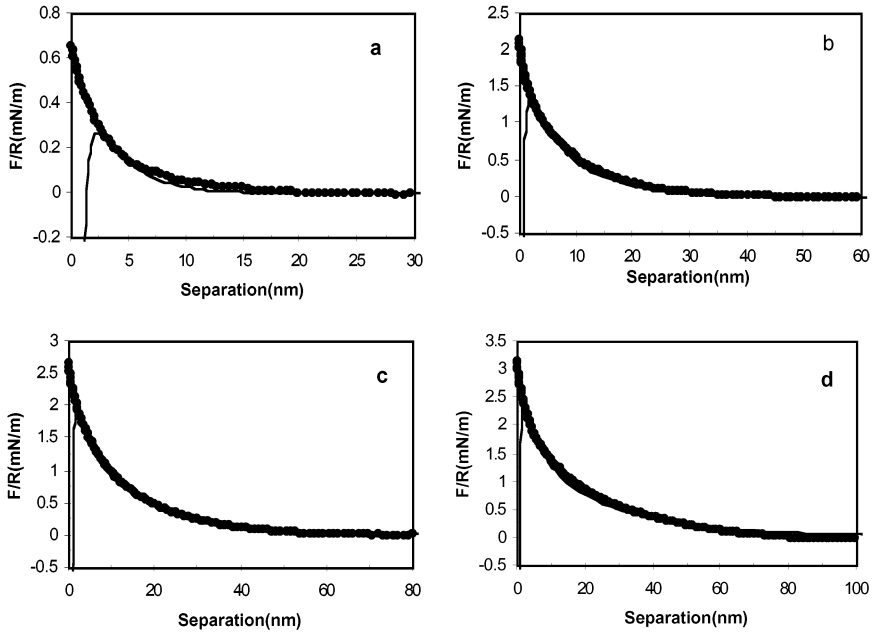

Figure 6. Measured (circles) and theoretical (solid lines) force between a silica sphere and Nafion film in $NaClO_4$ solutions of different concentrations. In each fit, $A_H = 1.0 \times 10^{-20}$ J, ψ_p = tip potential, ψ_s = substrate potential. (a) 10^{-2} M, $\psi_p = -20$ mV, $\psi_s = -14$ mV; (b) 10^{-3} M, $\psi_p = -40$ mV, $\psi_s = -40$ mV; (c) 3×10^{-4} M, $\psi_p = -60$ mV, $\psi_s = -64$ mV; (d) 10^{-4} M, $\psi_p = -90$ mV, $\psi_s = -88$ mV.

TABLE 1: Surface Potential and Surface Charge of Nafion Film in $NaClO_4$ Solution of Different Concentrations

c^s(mol/cm^3	ϕ_2 (V)	U_{IEM}[a]	$\sigma_{IEM} = -\sigma_{dl}$ (C/cm^2)
10^{-5}	−0.014	0.545	-3.23×10^{-7}
10^{-6}	−0.040	1.56	-3.19×10^{-7}
3×10^{-7}	−0.064	2.49	-3.24×10^{-7}
10^{-7}	−0.088	3.43	-3.15×10^{-7}

[a] Values of U_{IEM} computed from values of ϕ_2 assuming that $T =$ 298.2.

TABLE 2: Surface Potential and Surface Charge of Anion Exchange Membrane in Solutions of pH = 4 of Different Concentration

c^s(mol/cm^3	ϕ_2 (V)	U_{IEM}[a]	$\sigma_{IEM} = -\sigma_{dl}$ (C/cm^2)
10^{-5}	0.015	.584	-3.71×10^{-7}
10^{-6}	0.044	1.71	-3.58×10^{-7}
3×10^{-7}	0.070	2.72	-3.71×10^{-7}
10^{-7}	0.090	3.5	-3.645×10^{-7}

[a] Values of U_{IEM} computed from values of ϕ_2 assuming that $T =$ 298.2.

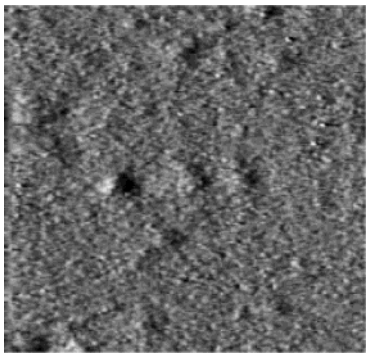

Figure 7. Atomic force microscopy image of PVF film.Scan area: 15×15 μm, Z-height: 100 nm.

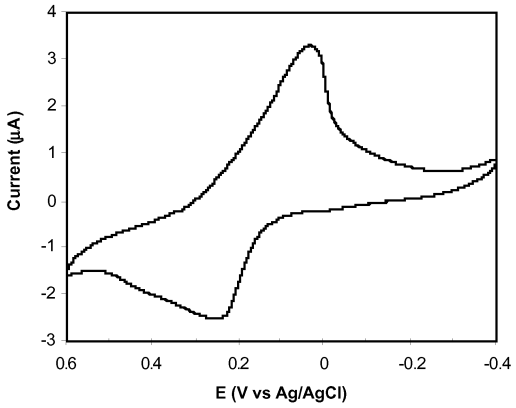

Figure 8. Cyclic voltammogram of PVF film in 10^{-4} M $HClO_4$ at a scan rate of 0.02 Vs^{-1}.

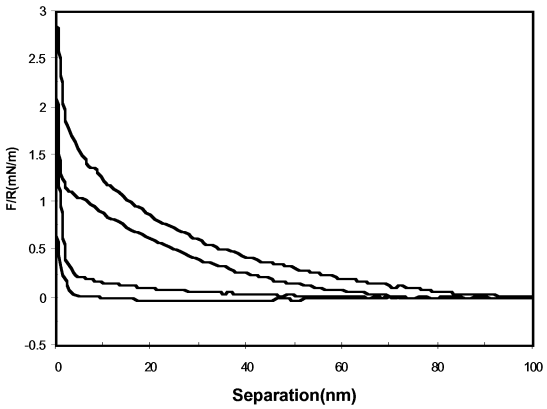

Figure 9. Forces between a positively charged polymer-sphere modified probe and the PVF film electrode as a function of electrode potential in 10^{-4} M $HClO_4$. The force curves correspond to controlled potentials of, from bottom to top, −0.4, −0.2, 0.2, 0.6 V vs Ag/AgCl.

Figure 9 shows the force curves between the positively charged polymer-sphere modified probe and the PVF film electrode as a function of electrode potential in 10^{-4} M $HClO_4$. At negative potentials, the PVF film is in the uncharged state, so there is no long distance electrostatic force between the positively charged probe and the PVF film. At shorter distances, the forces arising from possible compression of the tip double layer is compensated by attractive van der Waals forces. As

the potential increases, the PVF film becomes oxidized and positively charged. Since the AFM probe is positively charged, a repulsive force curve was obtained. As the potential became even more positive, the film was oxidized further and became more positively charged, leading to an increasing repulsive force.

For polymer films during electrochemical oxidation and reduction, there is a flux of ions into or out of the polymer film to compensate the charge in the film.[37,38] In a previous study, we reported that, for conjugated electronically conducting polymers (polythiophene and polypyrrole) there is a complete internal charge compensation in the polymer film and no diffuse double layer exists at the polymer film/solution interface. For the PVF film, which is a redox polymer that is not electronically conducting, potential-dependent force curves are obtained. Thus, for the PVF film, there is incomplete charge compensation within the film. The excess charge produces a diffuse double layer with the solution, as in metal or semiconductor electrodes. The reason for this qualitative difference between redox polymer (PVF) and conjugated conducting polymer (polythiophene and polypyrrole) is not clear. A possible explanation is the different structures of the polymer films. The redox polymer films are smooth and continuous, whereas the electronically conductive polymers tend to be more fibrous with nm-size pores or channels. Compensating ions can move into these nano channels and form internal double layers. As a consequence, the outer diffuse double layer becomes negligible compared to the internal ones and, therefore, are not sensed in AFM experiments. Another difference between redox and conjugated electronically conducting polymers (like polythiophene and polypyrrole) is that in the redox polymer like PVF there are fixed charges in its oxidized state while for the conducting polymer the charges are more delocalized.[39] Perhaps the existence of fixed charge plays a role in the formation of a diffuse double layer, as observed for the sulfonated polyaniline film.[28]

4. Discussion

The structure of an IEM is complicated. However, we do know that the density of charge sites within the membrane is large, of the order of 0.001 mol/cm^3. It will be adequate for our present puroses to assume that the potential drop between the bulk of the IEM and the IEM/solution interface, ϕ_m is small enough to be neglected and that the surface potential, ϕ_2 (see eq 1) comprises virtually the entire potential, V_{IEM}, between the bulk IEM and the bulk solution. To compute V_{IEM}, we assume that electroneutrality obtains in the bulk IEM and bulk electrolyte. Thus

$$c_1^{\,s} z_1 + c_2^s z_2 = 0 \tag{2}$$

and

$$c_0^m z_0 + c_1^m z_1 + c_2^m z_2 = 0 \tag{3}$$

where c_1^s and c_2^s are the concentrations of electrolyte species $s_1^{z_1}$ and $s_2^{z_2}$ in solution, c_1^m and c_2^m are the concentrations within the membrane, and c_0^m is the concentration of the immobilized charge within the IEM. To simplify the discussion, we assume that

$$z_1 = -z_2 = 1 \tag{4}$$

and

$$z_1 = -z_0 \tag{5}$$

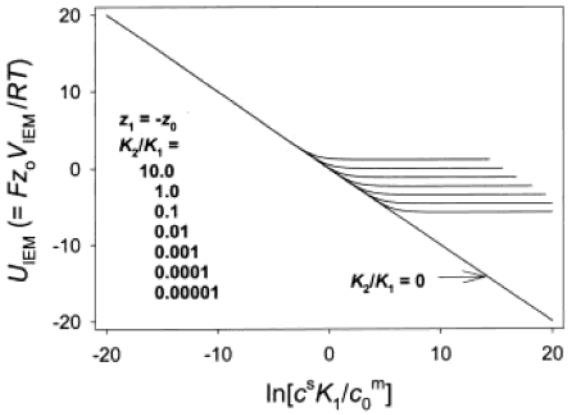

Figure 10. Plots of U_{IEM} vs $\ln(K_1 c^s/c_0^m)$computed from eq 11 for various values of K_2/K_1.

Thus, eq 2 becomes

$$c_1^s = c_2^s = c^s \tag{6}$$

and eq 2 becomes

$$c_0^m - c_1^m + c_2^m = 0 \tag{7}$$

The partitioning of the mobile species between the IEM and solution is described by

$$\frac{c_1^m}{c^s} = K_1 \exp\left[-\frac{Fz_1}{RT}V_{IEM}\right] = K_1 \exp\left[\frac{Fz_0}{RT}V_{IEM}\right] \tag{8}$$

and

$$\frac{c_2^m}{c^s} = K_2 \exp\left[-\frac{Fz_2}{RT}V_{IEM}\right] = K_2 \exp\left[-\frac{Fz_0}{RT}V_{IEM}\right] \tag{9}$$

where V_{IEM} is the potential of the bulk membrane vs the solution, and $K_{1,2} = \exp[(\mu_{1,2}^{o,s} - \mu_{1,2}^{o,m})/RT]$ and the μ^o-terms are the chemical potentials of $s_1^{z_1}$ or $s_2^{z_2}$ in the membrane or solution phase. Defining the normalized membrane potential U_{IEM} as

$$U_{IEM} = \frac{Fz_0}{RT}V_{IEM} = \frac{Fz_2}{RT}V_{IEM} = -\frac{Fz_1}{RT}V_{IEM} \tag{10}$$

we obtain, combining eqs 7−10

$$1 - \frac{K_1 c^s}{c_0^m}\left(\exp[U_{IEM}] - \frac{K_2}{K_1}\exp[-U_{IEM}]\right) = 0 \tag{11a}$$

$$\frac{K_1 c^s}{c_0^m} = [e^{U_{IEM}} + (K_2/K_1)e^{-U_{IEM}}]^{-1} \tag{11b}$$

A plot of U_{IEM} vs $\ln[K_1 c^s/c_o^m]$ for different values of K_2/K_1 is shown in Figure 10. A plot of the values of the experimental data for the Nafion film (Table 1) and for the anion exchange film is shown in Figure 11. For both films, we assume that $K_1/c_o^m = 3 \times 10^5$ cm^3/mol and $K_1 \simeq 300$. In both cases, it appears that $K_2/K_1 \approx 1$. These results should be viewed with caution because the experimental data for the highest electrolyte concentration, $c_s = 1 \times 10^{-5}$ mol/cm^3, is difficult to obtain because the diffuse layer is compact and because the forces are small. There are some satisfying features of this result:

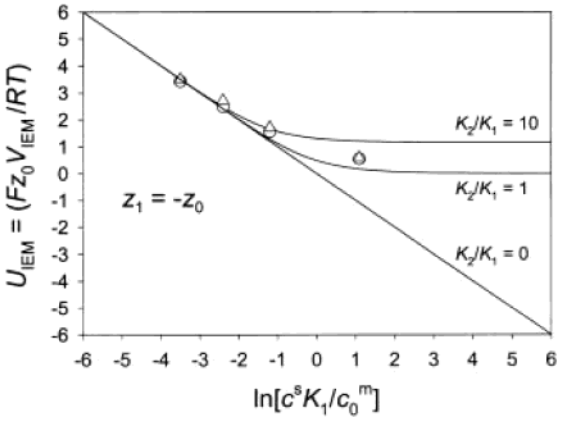

Figure 11. Plot of U_{IEM} vs $\ln(K_1c^s/c_0^m)$ for the Nafion (○) and for the anion (□) exchange membranes using data from Tables 1 and 2 and assuming that $K_1/c_0^m = 3 \times 10^5$ cm^3/mol.

1. It is reasonable that $K_2/K_1 \approx 1$ because the hydrophobicity of the anion and cation should not be vastly different. It is a bit surprising that K_1 is much greater than unity because one might expect that the operative dielectric constant within the IEM would be something less than ϵ_s (~78 for aqueous solutions). The result of assuming a smaller value of K_1 would be to effect a larger value of U_{IEM} than experimentally observed (see Figure 10). This could be reduced by assuming that some of the total interfacial potential is dropped across a capacitive region (the aforementioned equivalent of the Stern layer). For the present, we feel that the simplest analysis suffices. However, the experimental values of K_1 predict a deterioration in the permselectivity when $K_1c^s/c_o^m = 1$ or (if $c_o^m \simeq 0.001$ mol/cm^3, when $c_s \approx 3 \times 10^{-5}$ mol/cm^3), wich is lower than expected in Nafion.[40]

2. The experimentally measured charge in the diffuse layer (see Tables 1 and 2), deduced from the Gouy−Chapman expression (eq 1) is constant. This can be shown to be consistent with the theory under certain conditions. When $K_2/K_1 \exp[-2U_{IEM}] \ll 1$ (see eq 11). Equation 1 reduces to the familiar nernstian relationship

$$\frac{K_1c^s}{c_0^m} = \exp[-U_{IEM}] \tag{12}$$

and therefore

$$U_{IEM} = -\ln\left[\frac{K_1c^s}{c_0^m}\right] \tag{13}$$

We can now rewrite eq 1 as

$$\sigma^s = -\frac{z_0}{|z_0|}\sqrt{8RT\epsilon^s\epsilon_o c_s}\sinh\left[\frac{U_{IEM}}{2}\right] \tag{14}$$

Combining eqs 12 and 14 gives

$$\sigma^s = -\frac{z_0}{|z_0|}\sqrt{8RT\epsilon^s\epsilon_o c_s}\sinh\left[\frac{-\ln\left[\frac{K_1c_s}{c_0^m}\right]}{2}\right] \tag{15}$$

If a, is the argument of $\sinh[a]$ then $\sinh[a] \approx 1/2 \exp[a]$ when $\exp[2a] \gg 1$. Under these conditions, eq 15 reduces to

$$\sigma^s = -\frac{z_0}{2|z_0|}\sqrt{8RT\epsilon^s\epsilon_o c_s}\exp\left[\frac{-\ln\left[\frac{K_1c_s}{c_0^m}\right]}{2}\right] = -\frac{z_0}{2|z_0|}\sqrt{8RT\epsilon^s\epsilon_o c_0^m/K_1} \tag{16}$$

It is important to note that we have invoked the simplest theoretical analysis. A more complete approach would include an expression for the space charge within the IEM as well as consideration of an uncharged, purely capacitive region, analogous to the Stern layer in the traditional Gouy−Chapman−Stern model of an electrode/solution interface. Finally, we note that the Nafion film produced by coating from a solution will have properties somewhat different that a Nafion membrane.

5. Conclusions

The forces between colloidal probes and several polymer films (Nafion film, anion exchange membrane, and PVF film) were measured by AFM in the presence of a series of electrolyte solutions. Repulsive force was obtained at different concentrations of $NaClO_4$ for the Nafion film using a negatively charged silica tip. Similar results were obtained for an anion exchange membrane using a positively charged probe at solutions with pH 4. The surface charge density is independent of electrolyte concentration and the slope for a plot of potential drop vs $\ln[c^s]$ is ~0.020 V. A theoretical treatment based on GCS theory was employed to account for the above results. For a PVF film, potential-dependent force curves were obtained, which are qualitatively different from those of electronically conducting polymer film electrode.[1]

It should be noted that although the independence of the surface charge versus electrolyte concentration can be obtained in the proposed theoretical treatment for IEM, the surface charge density (~0.3μC/cm^2) seems to be a small value, which is much smaller than the value (more than 20μC/cm^2) for a highly charged surface. This phenomenon, which agrees with the results for bare Au electrode,[9] as we noted before, may imply that GCS theory is inadequate to describe solid/liquid interface, especially when applied to calculate the absolute value of the surface charge.

Acknowledgment. The support of this research by the National Science Foundation (CHE-0109587) and the Robert A. Welch Foundation is gratefully acknowledged. The authors thank Professor Andrew C. Hillier (University of Virginia) for developing the computer program for the calculation of double-layer forces.

References and Notes

(1) Wang, J.; Bard, A. J. *J. Am. Chem. Soc.* **2001**, *123*, 498.
(2) Adamson, A. W.; Gast, A. P. *Physical Chemistry of Surfaces*; John Wiley: London, 1997.
(3) *Electrical Phenomena at Interfaces: Fundamentals, Measurements, and Applications*; Ohshima, H.; Furusawa, K. Eds.; Marcel Dekker: New York, 1998.
(4) Hunter, R. J. *Foundations of Colloid Science*; Clarendon Press: London, 1989.
(5) *Handbook of Surface and Colloid Chemistry*; Birdi, Ed., CRC Press: New York, 1997; Chapter 11.
(6) Israelachvili, J. N. *Intermolecular and Surface Forces*, 2nd ed.; Academic Press: New York, 1991.
(7) Ducker, W. A.; Senden, T. J.; Pashley, R. M. *Nature* **1991**, *353*, 239.

(8) Butt, H.-J.; Jaschke, M.; Ducker, W. *Bioelectrochem. Bioenerg.* **1995**, *38*, 191.
(9) Wang, J.; Bard, A. J. *J. Phys. Chem.* **2001**, *105*, 5217.
(10) Hiller, A. C.; Kim, S.; Bard, A. J. *J. Phys. Chem.* **1996**, *100*, 18 808.
(11) (a) Israelachvili, J. N.; Adams, G. E. *J. Chem. Phys.* **1978**, *74*, 975. (b) Isrealachvili, J. N.; Adams, G. E. *J. Chem. Phys.* **1981**, *75*, 1400. (c) Fréchette, J.; Vanderlick, T. K. *Langmuir* **2001**, *17*, 7620.
(12) Ducker, W. A.; Senden, T.; Pashley, R. M. *Langmuir* **1992**, *8*, 1831.
(13) Veeramasunene, S.; Yalamanchili, M. R.; Miller, J. D. *J. Colloid Interface Sci.* **1996**, *184*, 594.
(14) Atkin, D. T.; Pashley, R. M. *Langmuir* **1993**, *9*, 412.
(15) Dedeloudis, C.; Fransaer J.; Celis, J.-P. *J. Phys. Chem.* **2000**, *104*, 2060.
(16) Atkins, D. T.; Pashley, R. M. *Langmuir* **1993**, *9*, 2232.
(17) Larson, I.; Drummond, C. J. Chan, D. Y. C.; Grieser, F. *J. Am. Chem. Soc.* **1993**, *115*, 11 885.
(18) Hu, K.; Fan, F.-R. F.; Bard, A. J.; Hillier, A. C. *J. Phys. Chem.* **1997**, *101*, 8298.
(19) Hu, K.; Bard, A. J. *Langmuir* **1997**, *13*, 5114.
(20) Kane, V.; Mulvaney, P. *Langmuir* **1998**, *14*, 3303.
(21) Hu, K.; Bard, A. J. *Langmuir* **1997**, *13*, 5418.
(22) Hu, K.; Pyat, R.; Bard, A. J. *Anal. Chem.* **1998**, *70*, 2870.
(23) Wang, J.; Bard, A. J. *Anal. Chem.* **2001**, *73*, 2207.
(24) Mulvaney, P.; Perera, J. M.; Biggs, S.; Grieser, F.; Stevens, G. W. *J. Colloid Interface Sci.* **1996**, *183*, 614.
(25) Meagher, L.; Pashley, R. M. *Langmuir* **1995**, *11*, 4019.
(26) Li, Y. Q.; Tao, N. J.; Pan, J.; Garcia, A. A.; Lindsay, S. M. *Langmuir* **1993**, *9*, 637.
(27) Hu, K.; Bard, A. J. *Chem. Mater.* **1998**, *10*, 1160.
(28) Campbell, S. D.; Hillier, A. C. *Langmuir* **1999**, *15*, 891.
(29) Derjaguin, B. *Trans. Faraday Soc.* **1940**, *36*, 203.
(30) Derjaguin, B. V.; Landau, L. D. *Acta Phys. Chem.* **1941**, *14*, 633.
(31) Derjaguin, B. V.; Landau, L. D. *J. Exp. Theor. Phys.* **1941**, *11*, 802.
(32) Verwey, E. J. W.; Overbeek, J. T. G. *Theory of the Stability of Lyophobic Colloids*; Elsevier: New York, 1948.
(33) Bard, A. J.; Faulkner, L. R. *Electrochemical Methods: Fundamentals and Applications*, 2nd ed.; John Wiley and Sons: New York, 2001; Chapter 13.
(34) James, P. J.; McMaster, T. J.; Newton, J. M.; Miles, M. J. *Polymer* **2000**, *41*, 4223.
(35) Meagher, L.; Pashley, R. M. *Langmuir* **1995**, *11*, 4019.
(36) Schroeder, A. H.; Kaufman, F. B.; Patel V.; Engler, E. M. *J. Electroanal. Chem.* **1980**, *113*, 193.
(37) Doblhofer, K In *Electrochemistry of Novel Materials*; Lipkowski, J., Ross, P. N., Eds.; VCH: New York, 1994.
(38) *Electroactive Polymer Electrochemistry*; Lyons M. E. G., Ed.; Plenum: New York, 1994.
(39) Doblhofer, K In *Handbook of Organic Conductive Molecules and Polymers*; Nalwa, H. S., Ed.; John Wiley and Sons: New York, 1997; Vol. 2.
(40) Pineri, M., Eisenberg, A., Eds. *Structure and Properties of Ionomers*; Reidel: Dordrecht, 1986.